ADVANCED MATERIALS
www.advmat.de

Complex Structures Made Simple – Continuous Flow Production of Core Cross-Linked Polymeric Micelles for Paclitaxel Pro-Drug-Delivery

Tobias A. Bauer, Jonas Schramm, Federico Fenaroli, Svenja Siemer, Christine I. Seidl, Christine Rosenauer, Regina Bleul, Roland H. Stauber, Kaloian Koynov, Michael Maskos, and Matthias Barz**

Translating innovative nanomaterials to medical products requires efficient manufacturing techniques that enable large-scale high-throughput synthesis with high reproducibility. Drug carriers in medicine embrace a complex subset of tasks calling for multifunctionality. Here, the synthesisof pro-drug-loaded core cross-linked polymeric micelles (CCPMs) in a continuous flow processis reported, which combines the commonly separated steps of micelle formation, core cross-linking, functionalization, and purification into a single process. Redox-responsive CCPMs are formed from thiol-reactive polypept(o)ides of polysarcosine-*block*-poly(*S*-ethylsulfonyl-L-cysteine) and functional cross-linkers based on dihydrolipoic acid hydrazide for pH-dependent release of paclitaxel. The precisely controlled microfluidic process allows the production of spherical micelles (D_h = 35 nm) with low polydispersity values (PDI < 0.1) while avoiding toxic organic solvents and additives with unfavorable safety profiles. Self-assembly and cross-linking via slit interdigital micromixers produces 350–700 mg of CCPMs/h per single system, while purification by online tangential flow filtration successfully removes impurities (unimer ≤ 0.5%). The formed paclitaxel-loaded CCPMs possess the desired pH-responsive release profile, display stable drug encapsulation, an improved toxicity profile compared to Abraxane (a trademark of Bristol-Myers Squibb), and therapeutic efficiency in the B16F1-xenotransplanted zebrafish model. The combination of reactive polymers, functional cross-linkers, and microfluidics enables the continuous-flow synthesis of therapeutically active CCPMs in a single process.

1. Introduction

Envisioning Paul Ehrlich's idea of the magic bullet, nanocarriers are designed to improve specificity, stability, and solubility of active pharmaceutical ingredients (APIs).[1–3] Due to their small size and high drug loading capacity, polymeric micelles have been thoroughly investigated for the delivery of small-molecule drugs such as anthracyclines and taxanes.[4–8] When nonspecific interactions are absent and a long half-life in the bloodstream permits slow accumulation in certain diseased tissues, e.g., solid tumors and granuloma, the more selective biodistribution of the encapsulated API can be achieved enabling higher maximum tolerated doses and improved therapeutic efficiency.[3,9–13] For targeted delivery and controlled release of APIs carrier disintegration and premature drug release immediately after the administration into the bloodstream need to be prevented, which require additional stabilization strategies.[14–16] Core cross-linked polymeric micelles (CCPMs) have thus evolved as the second

T. A. Bauer, C. I. Seidl, M. Barz
Leiden Academic Centre for Drug Research (LACDR)
Leiden University
Einsteinweg 55, Leiden 2333CC, The Netherlands
E-mail: m.barz@lacdr.leidenuniv.nl

J. Schramm, R. Bleul, M. Maskos
Fraunhofer Institute for Microengineering and Microsystems
Carl-Zeiss-Str. 18–20, 55129 Mainz, Germany

The ORCID identification number(s) for the author(s) of this article can be found under https://doi.org/10.1002/adma.202210704.

DOI: 10.1002/adma.202210704

F. Fenaroli
Department for Biosciences
University of Oslo
Blindernveien 31, 0371 Oslo, Norway

S. Siemer, R. H. Stauber
Molecular and Cellular Oncology/Nanobiomedicine
ENT Department
University Medical Center Mainz
Langenbeckstraße 1, 55131 Mainz, Germany

C. Rosenauer, K. Koynov
Max Planck Institute for Polymer Research
Ackermannweg 10, 55128 Mainz, Germany
E-mail: koynov@mpip-mainz.mpg.de

M. Barz
Department of Dermatology
University Medical Center of the Johannes Gutenberg University Mainz
Langenbeckstraße 1, 55131 Mainz, Germany

generation of polymeric micelles being stabilized in the core by covalent or strong noncovalent interactions.[16] Moreover, (bio-) reversible drug conjugation strategies allow for external or disease-related controlled drug release from CCPMs.[17–20] As the most promising example, CCPMs containing pH-cleavable docetaxel (CPC634) are currently under clinical evaluation for the treatment of platinum-resistant ovarian cancer in phase II (NCT03742713).[11,21,22]

The production of CCPMs typically involves the self-assembly of reactive block copolymers, cross-linking, (pro-) drug incorporation and purification, processes which require facile, robust, and scalable manufacturing.[23] The required reactive block copolymers commonly combine a functional block for chemoselective core cross-linking, by for, e.g., radical polymerization in the case of CriPEG (a trademark of Cristal Delivery BV) platform, with a stealth-like polymer block for steric shielding, mostly poly(ethylene glycol) (PEG).[11,21,22,24] In our case, we use a reactive copolymer completely based on endogenous amino acids, in which the stealth properties of polysarcosine (pSar) are combined with a poly(*S*-ethylsulfonyl-L-cysteine) (pCysSO_2Et) block allowing for bioreversible core-crosslinking by chemoselective disulfide formation.[25–27] Such polymers are known as polypept(o)ides and can be easily prepared by sequential living amine-initiated ring-opening *N*-carboxyanhydride (NCA) polymerization leading to well-defined polymers with narrow dispersity.[25–29] Polysarcosine, poly(*N*-methyl glycine), is hydrophilic, noncharged, and exclusively a weak hydrogen bond acceptor that adopts a random coil structure in aqueous solutions, meeting the characteristics for protein resistant materials.[30–32] Besides similar solution properties compared to PEG, pSar showed an improved safety profile, characterized by a reduced induction of cytokine release and evasion from accelerated blood clearance phenomenon.[30,33–35] The polypeptideL-CysSO_2Etenables secondary structure directed self-assembly and rapid (reaction rates: $k_{SH} >> 1\ s^{-1}$) chemo-selective core cross-linking by formation of asymmetric disulfides with di- or oligo-thiols providing control over particle morphology and functionality.[36–38]

While microfluidics have evolved to the state-of-the-art technique for the production of lipid nanoparticles (LNPs) and colloidal nanoparticles, polymeric micelles and in particular CCPMs are still synthesized in batch-mode using either film rehydration, solvent exchange, temperature-induced aggregation, or precipitation techniques.[39–45] In contrast to such methods, micromixers enable continuous-flow processes and offer automated manufacturing increasing production rates and reproducibility counteracting an advancing complexity, whereby the closed setup facilitates sterile particle preparation.[46,47] In the micrometer-sized compartments self-assembly can be tuned via solvents, temperature and concentrations, while diffusive mixing of the fluid streams governs the transfer of solvents or reagents, and can be adjusted for optimal particle size (hydrodynamic radius) and polydispersity index (PDI).[48–50] Mixing by simple T- or Y-junctions mainly leads to single and thick fluid lamellae resulting in high mixing times.[51] To reduce the mixing time and gain precise spatial and temporal control, interdigital micromixers have been developed. In the slit-interdigital micromixer (SIMM), multilamination and geometric flow focusing lead to thin fluid lamellae and high flow velocities.[51,52] The resulting short mixing times (ms-range) in interdigital micromixers can thus be used to control self-assembly kinetically, giving access to nonequilibrium structures as reported for micelles and disc-like structures from vesicle forming polymers by Thiermann et al.[46,49,53] Although microfluidics are an established technique for LNPs in nucleic acid delivery,[42,46,54–59] a complete setup for the continuous flow production of CCPMs including online purification has not yet been realized. The combination of self-assembly, core cross-linking and purification by this methodology is a highly desirable feature to enable larger-scale production and provide access to CCPM libraries for screening of drugs and combination therapies.[60,61]

Here, we now report the two-step synthesis and purification of functional CCPMs in a continuous flow process with online tangential flow filtration, whereby functional cross-linkers permit the decoupled and bio-reversible conjugation of a drugas demonstrated by the conjugation of a paclitaxel prodrug yielding drug-loaded CCPMs (PTX@CCPMs).

2. Results and Discussion

As illustrated in **Figure 1**A, block copolymers of polysarcosine-*block*-poly(*S*-ethylsulfonyl-L-cysteine) (pSar-*b*-pCys(SO_2Et)) are conventionally assembled to polymeric micelles by solvent switch methods. In a second step, the *S*-ethylsulfonyl-groups were addressed by rapid chemo-selective disulfide bond formation with thiols.[36,37] In this step, functional cross-linkers grant access to functional groups for bio-reversible drug conjugation, e.g., via pH-responsive hydrazone bonds, while the morphology of micelles is preserved due to the rapid disulfide formation between *S*-ethylsulfonyl-cysteines and dihydroxy lipoic acid derivatives (reaction rates: $k_{SH} >> 1\ s^{-1}$).[62] Conventional oxidative disulfide formation cannot provide the required rapid disulfide formation kinetics, which makes the use of *S*-ethylsulfonyl protective groups essential for the reported process.

The bottlenecks for the large-scale production of CCPMs by solution self-assembly are the concentration gradients for the crosslinker in large volumes, the considerable amount of time and solvent required for dialysis-based processes, and the purification of the product CCPMs from residual polymer and cross-linker via the laborious spin filtration procedure.

The continuous flow process for the production of therapeutically active CCPMs reported here addresses all the identified shortcomings by combining two slit interdigital micromixers with tangential flow filtration (Figure 1B) and enables the synthesis in a single step. As shown by the process chart in Figure 1C, self-assembly and core cross-linking were conducted in two consecutive micromixers connected to the online purification by tangential flow filtration. In the first step, the solution of the copolymer in the organic solvent (dimethylsulfoxide (DMSO)) is mixed with the block selective solvent (water). In the second micromixer, the cross-linker dissolved in ethanol/water mixtures is added to the micelle solution from micromixer #1. Since ethanol does not dissolve pCys(SO_2Et) the mixing step does not impair micelle integrity. For purification by tangential flow filtration regenerated cellulose membranes

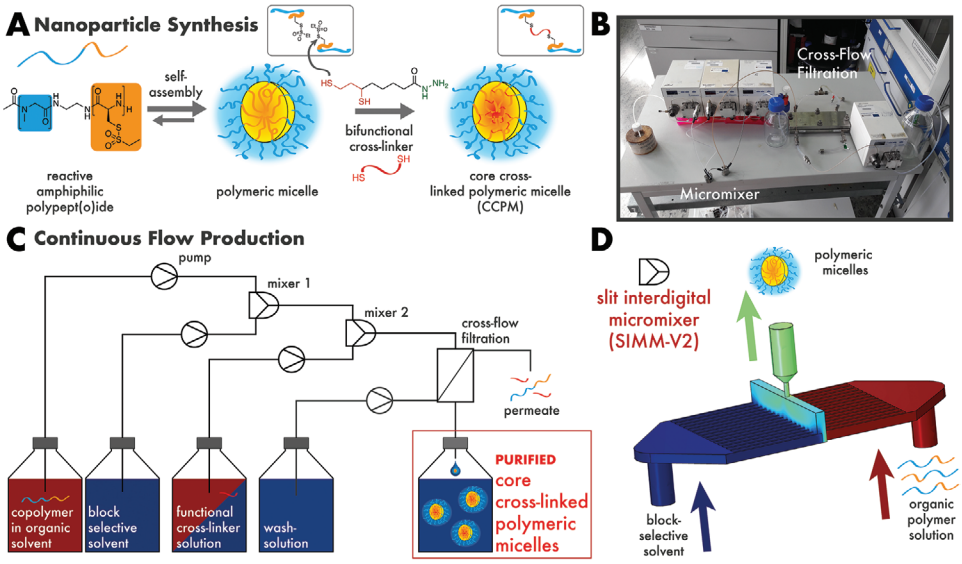

Figure 1. Synthesis of core cross-linked polymeric micelles in a continuous flow process. A) Amphiphilic thiol-reactive pSar-*b*-pCys(SO_2Et) polypept(o)ides are assembled to polymeric micelles via solvent switch followed by cross-linking by chemo-selective disulfide bond formation with dihydrolipoic acid hydrazide. B) Photo of the continuous flow setup. C) Chart of the continuous flow process. Reagent mixing by slit interdigital micromixers operated by HPLC pumps, and online particle purification by tangential flow filtration (MWCO, 30 kDa; regenerated cellulose membrane). D) Schematic illustration of the slit interdigital micromixer used for self-assembly and cross-linking (SIMM-V2).

(molecular weight cut-off (MWCO), 30 kDa) and water were employed yielding CCPMs in the retentate. The permeate (or waste) contains residual polymer, cross-linker, organic solvents, and tris(2-carboxyethyl)phosphine oxide, which was used to generate dihydrolipoic acid hydrazide from the parent disulfide. The dihydrolipoic acid hydrazide enables the covalent attachment of aldehyde or ketone containing drugs to the final CCPM.

The micromixer for self-assembly was directly connected to the one for the cross-linking step, and both were operated by conventional HPLC pumps. All mixing processes were performed in a slit-interdigital micromixer V2 (SIMM; Fraunhofer IMM), which allows for asymmetric flow ratios (e.g., 1–9), maintain a lamella structure without changes in thickness over a large variety of flow rates, and shows a low tendency for aggregate formation (Figure S2, Supporting Information). The SIMM splits the two fluid streams into eight lamellae fusing in an interdigital fashion (Figure 1D). The optimal overall flow rate was found to be ideal at 10–12 mL min^{-1} at which the microstructures (inner volume 8 µL) direct laminar flow at the beginning and rather turbulent flow near the outlet capillary after geometric flow focusing (outlet diameter 60 µm; Reynolds number ≈ 4500; total mixing time 40 ms). In comparison to the SIMM V2, a CAT mixer relies on dead volumes, which have very little flow, which may cause aggregation of block copolymer unimers. These aggregates can clog the mixer and end the continuous production process. To dissolve pSar-*b*-pCys(SO_2Et) copolymers DMSO was selected over *N*,*N*-dimethylacetamide (DMAc) used previously since the higher polymer solubility supports the formation of well-defined micelles (Figure S3, Supporting Information).[37,63,64] According to the guidelines of the International Council for Harmonization (ICH), DMSO and ethanol are classified as substances with a low toxic potential (class 3 solvent), allowing for a process without potentially hazardous solvents. In addition, the tangential flow filtration, removed remaining traces of cosolvents (no longer detectable by NMR RI or UV), non-crosslinked block copolymer and crosslinkers, yielding the final particle solution with a concentration of 14 g L^{-1}.

As shown in **Figure 2**, the micromixer process (MM) yielded polymeric micelles with small diameters (D_h = 34–36 nm) and narrow PDIs ≤ 0.1 at optimized conditions. Interestingly, the MM process does not require the presence of chaotropic thiourea for the formation of spherical micelles (+/− TU). The shear forces in the micromixer prevent the secondary structure directed self-assembly observed in solution, resulting in worm-like micelles referring to secondary structure-driven self-assembly of the pCys(SO_2Et) block.[37,63] Within the micromixer, the fast and precisely controlled solvent exchange thus governs the self-assembly process.[50,65] Consequently, small spherical nanoparticles were obtained from pSar-*b*-pCys(SO_2Et) in the micromixer that were identical to the CCPMs from the dialysis procedure with TU, in which antiparallel *β*-sheets were disrupted by saturation of the hydrogen bonds via the chaotropic agent.[37] Remarkably, cross-linking with dihydrolipoic acid hydrazide in SIMM #2 did not affect the particle size or PDI, as shown in Figure 2B (CCPM, W0). Moreover, the continuous flow process was robust to alterations in the polymer block lengths and in the relative flow rate ratios (Figure 2C; Figure S4, Supporting Information). For this setup up to 700 mg of CCPMs could be obtained per hour per micromixer system, whereby channel fouling was not observed at all. Since the microstructures are crucial for the performance of micromixers, a further scale-up can best be performed by parallelization, i.e., numbering up.[52] Purification of the CCPMs by tangential flow filtration slightly increased the particle diameter (39–48 nm),

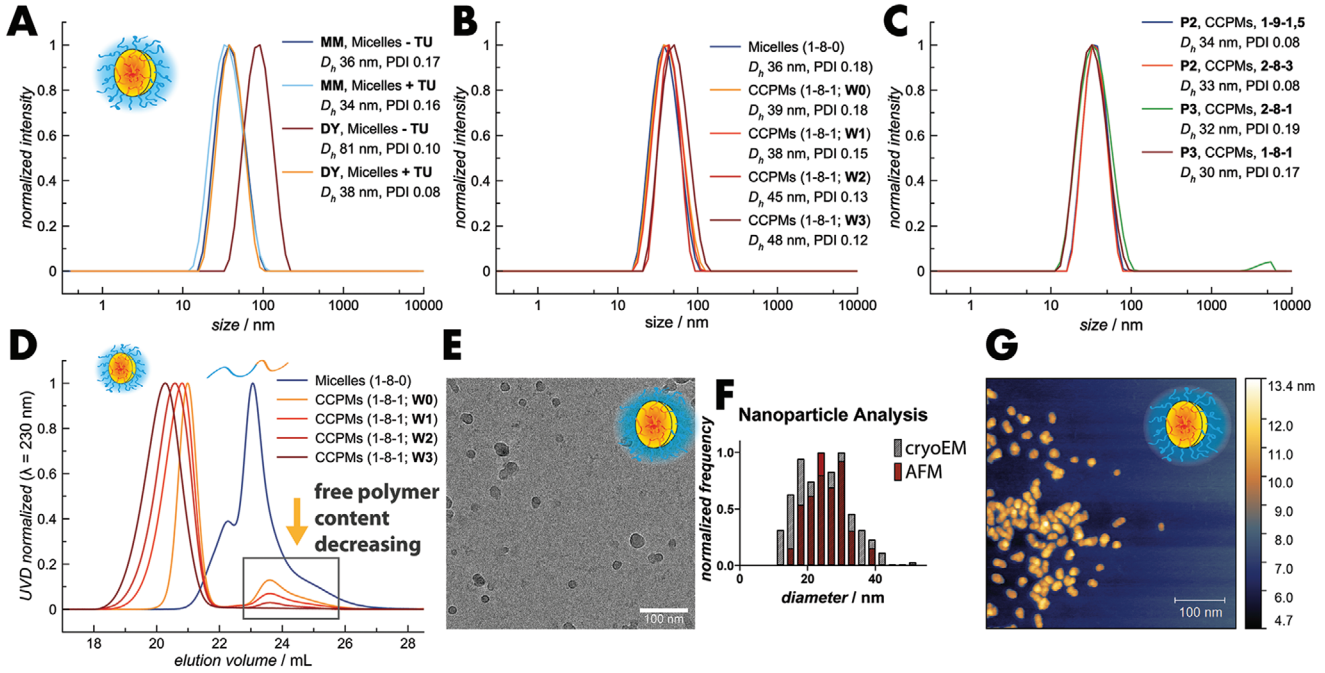

Figure 2. Analysis of micelles and CCPMs produced by continuous flow process. A) DLS analysis of micelles and CCPMs by self-assembly (DY) or micromixer process (MM) with or without thiourea (+/− TU). B) DLS analysis of micelles and CCPMs before (W0) and after purification by tangential filtration cycles (W1-W3). C) DLS analysis of CCPMs formed by varied relative flow rate ratios. D) HFIP-GPC analysis of micelles and CCPMs before and after purification by tangential-flow filtration cycles (W0–W3). E) Cryo-EM image of micromixer-CCPMs. F) Diameter of micromixer-CCPMs determined by AFM and cryo-EM image analysis. G) AFM image of micromixer-CCPMs.

while the PDI decreases. The tangential flow filtration ultimately led to CCPMs with free polymer contents below the limit of detection in HFIP-GPC analysis (≤0.5%) (Figure 2D; Figure S5, Supporting Information), which further underlines the stability of the CCPMs. Beyond small molecule contamination, purification from unconjugated polymer is of significance for most biomedical applications of CCPMs as free amphiphilic unimers cause unspecific interaction with plasma proteins.[66] Analysis of the CCPMs by cryogenic transmission electron microscopy (cryo-EM) and atomic force microscopy (AFM) confirmed the spherical morphology of the purified nanoparticles. The diameters of 24.8 ± 7.6 nm (cryo-EM) and 25.7 ± 5.3 nm (AFM) were in good agreement with (multiangle) DLS analysis, where no angle dependency was observed (Figure 2B,E–G; Figures S6–S9, Supporting Information). Interestingly, the formed CCPMs can not only be lyophilized and resuspended without alterations of the size distribution, but remain stable even as functional CCPMs over more than 3 years in solution (Figure S10, Supporting Information).

The presented continuous flow process successfully yielded CCPMs from pSar-*b*-pCys(SO_2Et) at varied chain lengths and flow rate ratios when the functional cross-linker dihydrolipoic acid hydrazide was used. In fact, the selection of the cross-linker was an important parameter for the process. If larger and more hydrophobic cross-linkers were used, aggregate formation and channel fouling were readily observed in the micromixer (Figures S11 and S12, Supporting Information). Moreover, the functional cross-linkers used in this study allowed the conjugation of multiple drugs to the given CCPM system. Each process can thus be optimized separately with the potential to achieve higher yields at reduced synthetic effort and cost.[67] Nevertheless, whenever lead compound have been identified drug loading can be easily implemented by adding a third micromixer.

As illustrated in **Figure 3**, the functional cross-linker lipoic acid hydrazide was designed to conjugate ketone-modified (pro) drugs to CCPMs by hydrazone bond formation, for example the PTX-LEV used here. Hydrazone bonds remain intact at physiological pH and enable stimuli-responsive drug release by cleavage at endo-lysosomal pH values.[19] In combination with the disulfide cross-links, PTX-loaded CCPMs (PTX@CCPMs) featured dual stimuli-responsive drug release accounting for optimal API delivery.[13] The contemporaneous availability of PTX and cysteine was not expected to interfere with the drug's mechanism of action but may be relevant for delivery of APIs such as cisplatin.[68,69]

Two techniques were evaluated for PTX conjugation to CCPMs: film-hydration and reaction in DMSO. For the latter, DMSO was employed to solubilize the drug and induce swelling of the micellar core. To provide an additional driving force for drug loading into the core, the film-hydration technique was adapted and modified from vesicle and micelle preparation methods. In both cases, excess PTX-LEV can be removed by centrifugation and filtration, and the final drug-loaded nanoparticles are obtained in aqueous solution after reconstitution with sterile water or buffer from lyophilization. The conjugation of PTX-LEV to lipoic acid hydrazide-functionalized CCPMs was verified by NMR analysis, whereby characteristic signals of the hydrazone-bond formation could be detected (Figure S13, Supporting Information). Further, both

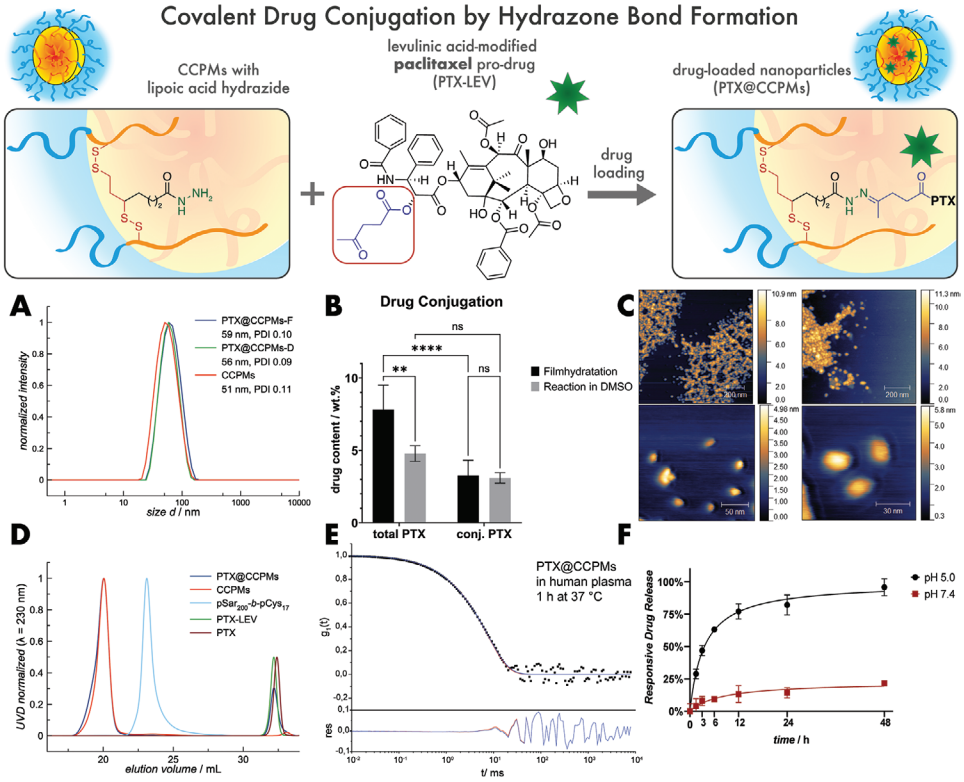

Figure 3. PTX pro-drug conjugation to functional CCPMs by hydrazone bond formation (PTX@CCPMs). A) DLS analysis showed narrow PDIs for CCPMs before and after drug loading, purification, lyophilization, and reconstitution in water. No significant differences were observed when film-hydration (PTX@CCPMs-F) or reaction in DMSO (PTX@CCPMs-D) were applied for drug conjugation. B) Quantification of total and conjugated amount of PTX (in wt%) by RP-HPLC. Data reported as N ± standard error of the mean for at least 4 independent experiments. Two-way ANOVA (*): *$p < 0.05$, **$p < 0.01$, ***$p < 0.001$, ****$p < 0.0001$. C) AFM images of PTX@CCPMs confirmed spherical particle morphology. D) HFIP-GPC analysis confirmed particle integrity after drug-loading. E) Multi angle DLS of PTX@CCPMs in undiluted human plasma: autocorrelation function $g_1(t)$ given for a representative measurement angle of 30°. The fits with (blue line) and without (red line) aggregation term (upper graph), and the derived residuals for the fit w/o aggregate (lower graph) indicated no significant deviation and thus no significant aggregation. F) Stimuli-responsive drug release at 37 °C in biologically relevant osmolar conditions (pH = 5.0 or 7.4), evaluated by RP-HPLC ($N = 3$).

loading techniques did not alter the narrow PDIs of below 0.1 for PTX@CCPMs (Figure 3A). In addition, the particle sizes were not significantly affected by the drug loading via film-hydration (PTX@CCPMs-F) or reaction in DMSO (PTX@CCPMs-D). As shown in Figure 3B, total paclitaxel contents of 7.81 ± 1.51 and 4.79 ± 0.47 wt% were determined for PTX@CCPMs-F and PTX@CCPM-D by RP-HPLC. Film-hydration thus leads to significantly higher total drug loading ($p < 0.0001$) compared to the reaction in DMSO. The comparable amounts of conjugated drug point toward a densely packed micellar core.[48,70] In fact, loading polymeric micelles with taxanes frequently leads to comparable or even lower drug contents of below 3 wt%.[71–73] When the conjugation reactions were performed in DMF or $CHCl_3$ which also solubilize the copolymer, no drug loading could be identified. In addition, reactions in DMSO in the presence of buffer containing aniline, which has been reported to catalyze the hydrazone bond formation for small molecules in solution, did not improve but decrease drug loading.[74,75] When analyzed by AFM, spherical structures with sizes well below 50 nm in diameter were revealed for PTX@CCPMs (Figure 3C). Drug loading did thus not affect the morphology of the nanoparticles. In addition, the GPC confirmed the integrity of the cross-linked nanomedicine, as no significant traces of homopolymer could be detected after incubation in HFIP for 1 h (Figure 3D).

For passive targeting of diseased tissue via the enhanced permeability and retention (EPR) effect or related phenomena, stable circulation in the blood stream without premature carrier disintegration and drug release is a basic requirement, which stimulated the development of CCPMs.[76] Unspecific interaction of the carrier with components of the blood plasma shall thus be prevented.[77] Consequently, PTX@CCPMs were analyzed by multi-angle DLS in human blood plasma following the procedure established by Rausch et al.[78] Here, no significant aggregation could be detected after incubation at 37 °C for 1 h (Figure 3E; Figure S14, Supporting Information).

To understand further the behavior of the CCPMs in human blood plasma we have labeled the micelles with a fluorescent dye (Atto647N) and studied them with fluorescence correlation spectroscopy (FCS).[79] Due to its very high sensitivity and fluorescence-based selectivity the method is uniquely suited for characterization of drug nanocarriers in undiluted blood plasma and even in whole blood.[80–82] The FCS experiments (Figure S15, Supporting Information) showed that after

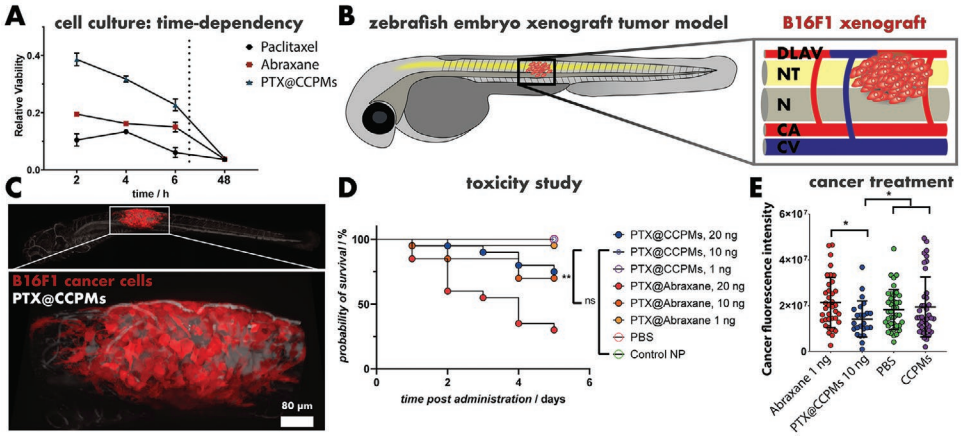

Figure 4. Biologic evaluation of PTX@CCPMs. A) Time-dependent toxicity of paclitaxel formulations in HeLa cells. B) Schematic illustration of the B16F1 mouse melanoma cell xenograft tumor model in zebrafish embryos. Cancer cells were injected in the neural tube which is located in the trunk region indicated by the black rectangle. The magnification shows neural tube (NT), noto-chord (N), dorsal longitudinal anastomotic vessel (DLAV), caudal artery (CA), and caudal vein (CV) with tumor formation after xenotransplantation in the neural tube.[85] C) Fluorescence microscopy image of the PTX@CCPM (white) accumulation in the tumor-region of RFP expressing B16F1 mouse melanoma cell (red) xenotransplanted zebrafish embryos, 8 h post nanoparticle injection. D) Toxicity study for paclitaxel formulations in zebrafish embryos (without tumor). $N \geq 20$. E) Cancer treatment study for paclitaxel formulations in B16F1 bearing zebrafish embryos. $N \geq 20$. Therapeutic dosis based on equal toxicity. The schematic illustration in (B) was adapted and modified from Kocere et al.[85]

incubation in undiluted human blood plasma at 37 °C for 1 h the CCPMs have a hydrodynamic radius $R_{H,plasma}$ = 31.3 nm, compared to $R_{H,water}$ = 30.7 nm measured in water. These basically identical values indicate that neither aggregation nor significant protein corona formation takes place in human blood plasma. Moreover, the autocorrelation curves of functional CCPMs remained identical at 0, 1, and 4 h incubation in plasma (Figure S16, Supporting Information).

The developed PTX@CCPMs displayed rapid drug release of 46.9 ± 3.2% after 3 h, and up to 95.8 ± 5.4% after incubation at pH 5 for 48 h. Vice versa, PTX@CCPMs are stable in PBS (pH 7.4), and only minor drug release of 7.9 ± 2.8% and 21.5 ± 1.1% could be detected after incubation over the same time frame (Figure S17, Supporting Information). This underlines the stimuli-responsive release mediated by the pH-sensitive hydrazone bone.[19,83,84]

Finally, the developed PTX@CCPMs were tested in cell culture and in zebrafish embryos, and their therapeutic performance was compared to Abraxane as internal reference (**Figure 4**). Abraxane is considered as the first FDA-approved nanomedicine, whereby PTX is formulated with human serum albumin replacing castor oil and ethanol used in Taxol.[86,87] As shown in Figure 4A, the time-dependent toxicity varied among the three formulations (Figure 4B) in HeLa (Figure S18, Supporting Information) and B16F10 (Figure S19, Supporting Information) cells. At equal drug concentration, free PTX in DMSO induced severe toxicity immediately. In contrast, Abraxane and PTX@CCPMs showed reduced toxicity after 2 h of treatment underlining the desired extracellular stability. Due to the pH drop during cellular uptake after 48 h incubation time, PTX@CCPMs and Abraxane showed similar IC_{50} values of 20.6 and 14.9×10^{-9} M in HeLa cells (Figure 4A), both comparable with the free drug dissolved in DMSO (11.7×10^{-9} M) (Figure S18, Supporting Information).[16] The identical cellular toxicity after 48 h, thus underlined efficient PTX release.

For the consequent in vivo study, we chose an established B16F1 melanoma zebrafish model. Zebrafish embryo are an emerging preclinical model allowing for rapid drug screening for novel therapeutic approaches against bacterial infections and cancer, substantially contributing to reducing animal testing in rodents.[12,85,88–90] In zebrafish embryo xenotransplanted with red fluorescent protein (RFP) expressing B16F1 mouse melanoma cells, PTX@CCPMs significantly accumulate in the tumor region within 8 h post injection according to fluorescence-based image analysis (Figure 4C; Figure S20, Supporting Information).[89,91] At this time point, more than 40% of the injected dose were still in circulation and could be detected in the vasculature (Figure S21 (Supporting Information); Figure 4C, upper image, PTX@CCPM in white). The drug loading did not impair the circulation behavior of the carrier but even slightly reduced nanoparticle clearance from the blood stream (Figure S21, Supporting Information). The maximum tolerated dose of PTX@CCPMs and Abraxane was tested using healthy zebrafish embryos (Figure 4D). For PTX@CCPMs, up to 10 ng of PTX per fish could be administered without detectable toxicity at day 5 post injection. In comparison, application of PTX via Abraxane was less well tolerated inducing toxicity even at lower doses (>1 ng). The more stable encapsulation of PTX by covalent conjugation in PTX@CCPMs thus reduces off-target toxicity of the taxane. These findings are in line with earlier reports on the reduced toxicity of doxorubicin encapsulated in polymersomes compared to the free drug tested in zebrafish embryos.[91] Ultimately, tumor therapy was performed at the maximal tolerated dose (MTD) using 10 and 1 ng PTX per fish administered by PTX@CCPMs or Abraxane compared to non-loaded CCPMs or PBS. As shown in Figure 4E, both PTX treatments showed a reduction in cancer growth, whereby PTX@CCPMs outperformed Abraxane at the MTD.

Taken together, the presented concept for the synthesis of drug-loaded CCPMs by continuous microfluidic processes

provides a convenient and highly controlled access to efficient nanomedicines. Future research will be directed to explore this platform beyond the model drug PTX and for encapsulation of synergistic APIs realizing combination therapy.

3. Conclusion

In this work, we report on a continuous flow process for the synthesis of functional core cross-linked polymeric micelles (CCPMs) allowing for precise control over the molecular properties of polymeric nanomedicines. The CCPMs are produced by self-assembly and cross-linking in two consecutive slit interdigital micromixers using chemo-selective disulfide bond formation of thiol-reactive polypept(o)ides (pSar-*b*-pCys(SO_2Et)) with functional cross-linkers. Online purification by tangential flow filtration was used for particle purification and could successfully reduce the amount of unconjugated polymer to below the limit of detection (≤0.5%). Without any numbering up by parallelization, the process leads to 350–700 mg CCPMs/h. Due to the precisely controlled self-assembly conditions, spherical micelles with a D_h = 35 nm and low PDI < 0.2 can be obtained. Consequently, the continuous flow process could be performed in solvents with a low toxicity profile (DMSO, ethanol) and aqueous buffer. Drug conjugation was demonstrated by paclitaxel-levulinic acid attachment to CCPMs via hydrazone bond formation (PTX@CCPMs). The drug-loading did not affect the nanoparticle size and morphology while featuring pH-responsive drug release. In cell culture (HeLa, B16F1) PTX@CCPMs showed similar performance compared to Abraxane, while the stable encapsulation in PTX@CCPMs reduced the toxicity of the paclitaxel and allowed for higher dosing in a zebrafish xenograft model (B16F1). In this model, PTX@CCPMs outperform Abraxane in therapeutic efficiency underlining the potential of CCPMs containing covalently attached taxanes. In addition, the presented strategy enables the attachment of multiple drugs required for the rapid development of combination therapies. The presented continuous flow process for the production and purification will ease this development substantially and foster the translation of CCPMs by enabling the straightforward synthesis of particle libraries under precisely controlled conditions.

Supporting Information

Supporting Information is available from the Wiley Online Library or from the author.

Acknowledgements

The authors acknowledge Holger Adam for AFM support. The authors thank Helma Burg and Rüdiger Berger (both Max Planck Institute for Polymer Research, Physics at Interfaces) for performing additional AFM measurements and providing the data for some samples. The authors also thank the Netherlands Centre for Electron Nanoscopy for the access and Dr. Willem Noteborn for cryo-EM measurements. T.A.B. would like to thank the HaVo Stiftung and the Max-Planck-Graduate-Center for financial support. T.A.B., C.I.S., M.M., K.K., and M.B. acknowledge the Deutsche Forschungsgemeinschaft (SFB1066) for funding.

Conflict of Interest

The authors declare no conflict of interest.

Data Availability Statement

The data that support the findings of this study are available from the corresponding author upon reasonable request.

Keywords

cross-linking, microfluidics, nanomedicine, polymeric micelles, polypept(o)ides

Received: November 17, 2022
Revised: February 10, 2023
Published online: April 6, 2023

[1] N. Bertrand, J. C. Leroux, *J. Controlled Release* **2012**, *161*, 152.
[2] T. Lammers, *Int. J. Pharm.* **2013**, *454*, 527.
[3] T. Lammers, F. Kiessling, W. E. Hennink, G. Storm, *J. Controlled Release* **2012**, *161*, 175.
[4] H. Cabral, K. Miyata, K. Osada, K. Kataoka, *Chem. Rev.* **2018**, *118*, 6844.
[5] M. Murakami, H. Cabral, Y. Matsumoto, S. Wu, M. R. Kano, T. Yamori, N. Nishiyama, K. Kataoka, *Sci. Transl. Med.* **2011**, *3*, 64ra2.
[6] M. Talelli, M. Iman, A. K. Varkouhi, C. J. F. Rijcken, R. M. Schiffelers, T. Etrych, K. Ulbrich, C. F. van Nostrum, T. Lammers, G. Storm, W. E. Hennink, *Biomaterials* **2010**, *31*, 7797.
[7] D. D. Von Hoff, M. M. Mita, R. K. Ramanathan, G. J. Weiss, A. C. Mita, P. M. Lorusso, H. A. Burris, L. L. Hart, S. C. Low, D. M. Parsons, S. E. Zale, J. M. Summa, H. Youssoufian, J. C. Sachdev, *Clin. Cancer Res.* **2016**, *22*, 3157.
[8] H. Mukai, K. Kato, T. Esaki, S. Ohsumi, Y. Hozomi, N. Matsubara, T. Hamaguchi, Y. Matsumura, R. Goda, T. Hirai, Y. Nambu, *Invest New Drugs* **2016**, *34*, 750.
[9] Y. Matsumura, H. Maeda, *Cancer Res.* **1986**, *46*, 6387.
[10] H. Maeda, *J. Controlled Release* **2012**, *164*, 138.
[11] F. Atrafi, R. A. G. van Eerden, M. A. M. van Hylckama Vlieg, E. Oomen-de Hoop, P. de Bruijn, M. P. Lolkema, A. Moelker, C. J. Rijcken, R. Hanssen, A. Sparreboom, F. A. L. M. Eskens, R. H. J. Mathijssen, S. L. W. Koolen, *Clin. Cancer Res.* **2020**, *26*, 3537.
[12] F. Fenaroli, U. Repnik, Y. Xu, K. Johann, S. Van Herck, P. Dey, F. M. Skjeldal, D. M. Frei, S. Bagherifam, A. Kocere, R. Haag, B. G. De Geest, M. Barz, D. G. Russell, G. Griffiths, *ACS Nano* **2018**, *12*, 8646.
[13] R. A. G. Van Eerden, R. H. J. Mathijssen, S. L. W. Koolen, *Int. J. Nanomed.* **2020**, *15*, 8151.
[14] J. Lu, S. C. Owen, M. S. Shoichet, *Macromolecules* **2011**, *44*, 6002.
[15] W. Richtering, I. Alberg, R. Zentel, *Small* **2020**, *16*, 2002162.
[16] M. Talelli, M. Barz, C. J. F. F. Rijcken, F. Kiessling, W. E. Hennink, T. Lammers, *Nano Today* **2015**, *10*, 93.
[17] Z. Su, Y. Liang, Y. Yao, T. Wang, N. Zhang, *J. Mater. Chem. B* **2016**, *4*, 1122.
[18] C. J. Rijcken, C. J. Snel, R. M. Schiffelers, C. F. van Nostrum, W. E. Hennink, *Biomaterials* **2007**, *28*, 5581.
[19] S. J. Sonawane, R. S. Kalhapure, T. Govender, *Eur. J. Pharm. Sci.* **2017**, *99*, 45.
[20] T. A. Bauer, J. Eckrich, N. Wiesmann, F. Kuczelinis, W. Sun, X. Zeng, B. Weber, S. Wu, N. H. Bings, S. Strieth, M. Barz, *J. Mater. Chem. B* **2021**, *9*, 8211.

[21] Q. Hu, C. J. Rijcken, R. Bansal, W. E. Hennink, G. Storm, J. Prakash, *Biomaterials* **2015**, *53*, 370.
[22] I. Biancacci, Q. Sun, D. Möckel, F. Gremse, S. Rosenhain, F. Kiessling, M. Bartneck, Q. Hu, M. Thewissen, G. Storm, W. E. Hennink, Y. Shi, C. J. F. Rijcken, T. Lammers, A. M. Sofias, *J. Controlled Release* **2020**, *328*, 805.
[23] M. Barz, *Nanomedicine* **2015**, *10*, 3093.
[24] F. Atrafi, R. A. G. van Eerden, S. L. W. Koolen, P. de Bruijn, C. J. F. Rijcken, R. Hanssen, F. A. L. M. Eskens, M. P. Lolkema, E. Oomen-de Hoop, J. Damman, R. H. J. Mathijssen, *Cancers (Basel)* **2021**, *13*, 3741.
[25] A. Birke, D. Huesmann, A. Kelsch, M. Weilbächer, J. Xie, M. Bros, T. Bopp, C. Becker, K. Landfester, M. Barz, *Biomacromolecules* **2014**, *15*, 548.
[26] A. Birke, J. Ling, M. Barz, *Prog. Polym. Sci.* **2018**, *81*, 163.
[27] K. Klinker, M. Barz, *Macromol. Rapid Commun.* **2015**, *36*, 1943.
[28] T. Aliferis, H. Iatrou, N. Hadjichristidis, *Biomacromolecules* **2004**, *5*, 1653.
[29] C. Fetsch, A. Grossmann, L. Holz, J. F. Nawroth, R. Luxenhofer, *Macromolecules* **2011**, *44*, 6746.
[30] B. Weber, A. Birke, K. Fischer, M. Schmidt, M. Barz, *Macromolecules* **2018**, *51*, 2653.
[31] E. Ostuni, R. G. Chapman, R. E. Holmlin, S. Takayama, G. M. Whitesides, *Langmuir* **2001**, *17*, 5605.
[32] K. H. A. Lau, C. Ren, T. S. Sileika, S. H. Park, I. Szleifer, P. B. Messersmith, *Langmuir* **2012**, *28*, 16099.
[33] B. Weber, C. Seidl, D. Schwiertz, M. Scherer, S. Bleher, R. Süss, M. Barz, *Polymers (Basel)* **2016**, *8*, 427.
[34] S. S. Nogueira, A. Schlegel, K. Maxeiner, B. Weber, M. Barz, M. A. Schroer, C. E. Blanchet, D. I. Svergun, S. Ramishetti, D. Peer, P. Langguth, U. Sahin, H. Haas, *ACS Appl. Nano Mater.* **2020**, *3*, 10634.
[35] K. Son, M. Ueda, K. Taguchi, T. Maruyama, S. Takeoka, Y. Ito, *J. Controlled Release* **2020**, *322*, 209.
[36] O. Schäfer, K. Klinker, L. Braun, D. Huesmann, J. Schultze, K. Koynov, M. Barz, *ACS Macro Lett.* **2017**, *6*, 1140.
[37] K. Klinker, O. Schäfer, D. Huesmann, T. Bauer, L. Capelôa, L. Braun, N. Stergiou, M. Schinnerer, A. Dirisala, K. Miyata, K. Osada, H. Cabral, K. Kataoka, M. Barz, *Angew. Chem., Int. Ed.* **2017**, *56*, 9608.
[38] D. Huesmann, O. Schäfer, L. Braun, K. Klinker, T. Reuter, M. Barz, *Tetrahedron Lett.* **2016**, *57*, 1138.
[39] Y. Liu, G. Yang, Y. Hui, S. Ranaweera, C. X. Zhao, *Small* **2022**, *18*, 2106580.
[40] S. Marre, K. F. Jensen, *Chem. Soc. Rev.* **2010**, *39*, 1183.
[41] Y. Mai, A. Eisenberg, *Chem. Soc. Rev.* **2012**, *41*, 5969.
[42] H. Zhang, Y. Zhu, Y. Shen, *Small* **2018**, *14*, 1800360.
[43] J. M. Lim, N. Bertrand, P. M. Valencia, M. Rhee, R. Langer, S. Jon, O. C. Farokhzad, R. Karnik, *Nanomed. Nanotechnol. Biol. Med.* **2014**, *10*, 401.
[44] S. Battat, D. A. Weitz, G. M. Whitesides, *Lab Chip* **2022**, *22*, 530.
[45] M. J. W. Evers, J. A. Kulkarni, R. van der Meel, P. R. Cullis, P. Vader, R. M. Schiffelers, *Small Methods* **2018**, *2*, 1700375.
[46] B. K. Johnson, R. K. Prud'homme, *Phys. Rev. Lett.* **2003**, *91*, 118302.
[47] Y. Dou, B. Wang, M. Jin, Y. Yu, G. Zhou, L. Shui, *J. Micromech. Microeng.* **2017**, *27*, 113002.
[48] Z. L. Tyrrell, Y. Shen, M. Radosz, *Prog. Polym. Sci.* **2010**, *35*, 1128.
[49] R. Bleul, R. Thiermann, M. Maskos, *Macromolecules* **2015**, *48*, 7396.
[50] S. Keßler, K. Drese, F. Schmid, *Polymer (Guildf)* **2017**, *126*, 9.
[51] D. Ziegenbalg, C. Kompter, F. Schönfeld, D. Kralisch, *Green Process. Synth.* **2012**, *1*, 211.
[52] C. Tonhauser, A. Natalello, H. Löwe, H. Frey, *Macromolecules* **2012**, *45*, 9551.
[53] R. Thiermann, R. Bleul, M. Maskos, *Macromol. Chem. Phys.* **2017**, *218*, 1600347.
[54] L. Schoenmaker, D. Witzigmann, J. A. Kulkarni, R. Verbeke, G. Kersten, W. Jiskoot, D. J. A. Crommelin, *Int. J. Pharm.* **2021**, *601*, 120586.
[55] D. Chen, K. T. Love, Y. Chen, A. A. Eltoukhy, C. Kastrup, G. Sahay, A. Jeon, Y. Dong, K. A. Whitehead, D. G. Anderson, *J. Am. Chem. Soc.* **2012**, *134*, 6948.
[56] M. Rhee, P. M. Valencia, M. I. Rodriguez, R. Langer, O. C. Farokhzad, R. Karnik, *Adv. Mater.* **2011**, *23*, H79.
[57] L. Capretto, D. Carugo, W. Cheng, M. Hill, X. Zhang, *J. Colloid Interface Sci.* **2011**, *357*, 243.
[58] N. M. Belliveau, J. Huft, P. J. Lin, S. Chen, A. K. Leung, T. J. Leaver, A. W. Wild, J. B. Lee, R. J. Taylor, Y. K. Tam, C. L. Hansen, P. R. Cullis, *Mol. Ther. Nucleic Acids* **2012**, *1*, e37.
[59] S. von Bomhard, J. Schramm, R. Bleul, R. Thiermann, P. Höbel, U. Krtschil, P. Löb, M. Maskos, *Chem. Eng. Technol.* **2019**, *42*, 2085.
[60] F. Greco, M. J. Vicent, *Adv. Drug Delivery Rev.* **2009**, *61*, 1203.
[61] S. Siemer, T. A. Bauer, P. Scholz, C. Breder, F. Fenaroli, G. Harms, D. Dietrich, J. Dietrich, C. Rosenauer, M. Barz, S. Becker, S. Strieth, C. Reinhardt, T. Fauth, J. Hagemann, R. H. Stauber, *ACS Nano* **2021**, *15*, 18541.
[62] O. Schäfer, D. Huesmann, C. Muhl, M. Barz, *Chem. – A Eur. J.* **2016**, *22*, 18085.
[63] T. A. Bauer, J. Imschweiler, C. Muhl, B. Weber, M. Barz, *Biomacromolecules* **2021**, *22*, 2171.
[64] N. E. Clay, J. J. Whittenberg, J. Leong, V. Kumar, J. Chen, I. Choi, E. Liamas, J. M. Schieferstein, J. H. Jeong, D. H. Kim, Z. J. Zhang, P. J. A. Kenis, I. W. Kim, H. Kong, *Nanoscale* **2017**, *9*, 5194.
[65] R. Thiermann, R. Bleul, M. Maskos, *Macromol. Chem. Phys.* **2017**, *218*, 1600347.
[66] I. Alberg, S. Kramer, C. Leps, S. Tenzer, R. Zentel, *Macromol. Biosci.* **2021**, *21*, 2000414.
[67] T. Ojha, Q. Hu, C. Colombo, J. Wit, M. Geijn, M. J. Steenbergen, M. Bagheri, H. Königs-Werner, E. M. Buhl, R. Bansal, Y. Shi, W. E. Hennink, G. Storm, C. J. F. Rijcken, T. Lammers, *Biotechnol. J.* **2021**, *16*, 2000212.
[68] Y. K. Lee, S. Y. Han, Y. W. Chin, Y. H. Choi, *Arch. Pharm. Res.* **2012**, *35*, 509.
[69] L. Galluzzi, L. Senovilla, I. Vitale, J. Michels, I. Martins, O. Kepp, M. Castedo, G. Kroemer, *Oncogene* **2012**, *31*, 1869.
[70] J. Gou, S. Feng, H. Xu, G. Fang, Y. Chao, Y. Zhang, H. Xu, X. Tang, *Biomacromolecules* **2015**, *16*, 2920.
[71] Z. L. Tyrrell, Y. Shen, M. Radosz, *J. Phys. Chem. C* **2011**, *115*, 11951.
[72] J. Logie, A. N. Ganesh, A. M. Aman, R. S. Al-awar, M. S. Shoichet, *Biomaterials* **2017**, *123*, 39.
[73] K. M. Huh, S. C. Lee, Y. W. Cho, J. Lee, J. H. Jeong, K. Park, *J. Controlled Release* **2005**, *101*, 59.
[74] D. Larsen, A. M. Kietrys, S. A. Clark, H. S. Park, A. Ekebergh, E. T. Kool, *Chem. Sci.* **2018**, *9*, 5252.
[75] S. Morales, J. L. Aceña, J. L. García Ruano, M. B. Cid, *J. Org. Chem.* **2016**, *81*, 10016.
[76] R. Van Der Meel, E. Sulheim, Y. Shi, F. Kiessling, W. J. M. Mulder, *Nat. Nanotechnol.* **2019**, *14*, 1007.
[77] I. Alberg, S. Kramer, M. Schinnerer, Q. Hu, C. Seidl, C. Leps, N. Drude, D. Möckel, C. Rijcken, T. Lammers, M. Diken, M. Maskos, S. Morsbach, K. Landfester, S. Tenzer, M. Barz, R. Zentel, *Small* **2020**, *16*, 1907574.
[78] K. Rausch, A. Reuter, K. Fischer, M. Schmidt, *Biomacromolecules* **2010**, *11*, 2836.
[79] R. Rigler, E. S. Elson, *Fluorescence Correlation Spectroscopy: Theory and Applications*, Springer, Berlin Heidelberg, **2012**.
[80] S. Schmitt, L. Nuhn, M. Barz, H. Butt, K. Koynov, *Macromol. Rapid Commun.* **2022**, *43*, 2100892.
[81] I. Negwer, A. Best, M. Schinnerer, O. Schäfer, L. Capeloa, M. Wagner, M. Schmidt, V. Mailänder, M. Helm,

M. Barz, H.-J. Butt, K. Koynov, *Nat. Commun.* **2018**, *9*, 5306.
[82] S. Schmitt, A. Huppertsberg, A. Klefenz, L. Kaps, V. Mailänder, D. Schuppan, H. J. Butt, L. Nuhn, K. Koynov, *Biomacromolecules* **2022**, *23*, 1065.
[83] Y. Shi, C. F. Van Nostrum, W. E. Hennink, *ACS Biomater. Sci. Eng.* **2015**, *1*, 393.
[84] Y. Bae, N. Nishiyama, S. Fukushima, H. Koyama, M. Yasuhiro, K. Kataoka, *Bioconjug. Chem.* **2005**, *16*, 122.
[85] A. Kocere, J. Resseguier, J. Wohlmann, F. M. Skjeldal, S. Khan, M. Speth, N. K. Dal, M. Y. W. Ng, N. Alonso-Rodriguez, E. Scarpa, L. Rizzello, G. Battaglia, G. Griffiths, F. Fenaroli, *EBioMedicine* **2020**, *58*, 102902.
[86] D. A. Yardley, *J. Controlled Release* **2013**, *170*, 365.
[87] E. Miele, G. P. Spinelli, E. Miele, F. Tomao, S. Tomao, *Int. J. Nanomed.* **2009**, *4*, 99.
[88] S. Sieber, P. Grossen, P. Detampel, S. Siegfried, D. Witzigmann, J. Huwyler, *J. Controlled Release* **2017**, *264*, 180.
[89] N. K. Dal, A. Kocere, J. Wohlmann, S. Van Herck, T. A. Bauer, J. Resseguier, S. Bagherifam, H. Hyldmo, M. Barz, B. G. De Geest, F. Fenaroli, *Small* **2020**, *16*, 1906719.
[90] S. Cassar, I. Adatto, J. L. Freeman, J. T. Gamse, I. Iturria, C. Lawrence, A. Muriana, R. T. Peterson, S. Van Cruchten, L. I. Zon, *Chem. Res. Toxicol.* **2020**, *33*, 95.
[91] A. Kocere, J. Resseguier, J. Wohlmann, F. M. Skjeldal, S. Khan, M. Speth, N.-J. K. Dal, M. Y. W. Ng, N. Alonso-Rodriguez, E. Scarpa, L. Rizzello, G. Battaglia, G. Griffiths, F. Fenaroli, *EBioMedicine* **2020**, *58*, 102902.